Mechanical and Structural Properties of Melt Spun Polypropylene/nylon 6 Alloy Filaments

Mehdi Afshari,[1] Richard Kotek,[2] Bhupender S. Gupta,[2] Mohammad Haghighat Kish,[3] Hosein Nazock Dast[4]

[1]*Department of Textile Engineering, Yazd University, P. O. Box 89195–741, Yazd, Iran*
[2]*College of Textiles, Textile Engineering, Chemistry and Science Engineering, North Carolina State University, Box 8301, Raleigh, North Carolina 27695, USA*
[3]*Department of Textile Engineering, Amir Kabir University of Technology, P. O. Box 15875-4413, Tehran, Iran*
[4]*Department of Polymer Engineering, Amir Kabir University of Technology, P. O. Box 15875-4413, Tehran, Iran*

Received 16 April 2004; accepted 6 December 2004
DOI 10.1002/app.21772
Published online in Wiley InterScience (www.interscience.wiley.com).

ABSTRACT: Investigated in the present study are the physical properties, morphology, and structure of PP/N6 alloy filaments (10, 20 wt % N6) made with or without PP-*g*-MAH as compatibilizer. The alloy filaments produced at the take-up speeds of 300 and 800 m/min were drawn with draw ratio of 3.5 and 2, respectively. Stress–strain curves of PP and alloy filaments show ductile and brittle behavior, respectively. It is suggested that the brittle behavior of alloy filaments is due to the presence of microvoids or micropores at the interface of PP and N6; these lead to stress concentration and thus to a decrease in tenacity, modulus, and elongation at break. Effects of the blending of N6 with PP on birefringence and crystalline and amorphous orientation factors of the composite filaments are studied. The amorphous orientation factor, f_{am}, of PP was found to increase with an increase in the amount of N6. The alloy filaments behaved like isostrain materials and most of the force in spinning and drawing was born by the PP phase. The presence of N6 fibrils helped to orient PP chain molecules in amorphous regions. However, the crystalline factor, f_c, of PP decreased with the increase in nylon fraction. This means the presence of the crystals of N6 caused a decrease in the orientation of the PP crystals. LSCM micrographs of the filament showed the presence of matrix–fibril morphology with the N6 fibrils oriented along the axis. © 2005 Wiley Periodicals, Inc. J Appl Polym Sci 97: 532–544, 2005

Key words: polypropylene; nylon; alloys; orientation

INTRODUCTION

The purpose of blending polymers is to obtain materials with additional properties with minimum sacrifice in original properties.[1,2] An immiscible blended polymer system usually has a microstructure with the phase separation between components. This system is, therefore, a new polymeric material with special features of each polymer. In immiscible polymer blends, the major component forms a continuous matrix while the disperse component assumes different forms (droplet, rod, fibril, or lamella).[3] For improving strength and stability of the interface in the immiscible polymer blends, interface modifiers are added.[4]

It has been reported that melt spinning of immiscible polymer blends into fibers is of great interest to the industry as synthetic fibers containing improved properties could be produced.[5]

Production of polypropylene (PP) fibers has increased at an accelerated rate due to the simplicity of the production technology involved and the valuable properties the fiber possesses: very low density, chemical resistance, and sufficiently high physicomechanical characteristics, including high resistance to wear. Blends of PP and nylon 6 (N6) have received much attention in recent years.[6] PP and N6 are immiscible polymers that, when combined, lead to materials with improved chemical and mechanical characteristics. PP-*g*-MAH has been shown to be an effective compatibilizer for the system.[7] The elongation force field in the melt spinning process has been found to be more effective in producing fibrillar morphology than the shear force field present in the extrusion and molding processes.[8]

Takahashi and coworkers[9] studied the effect of viscosity ratio (the ratio of the viscosity of PP to that of N6) on the structure of PP/N6 fibers. They proposed that, for a polyblend fiber having a viscosity ratio greater than 1, the crystal orientation of PP was considerably lower than that observed when the viscosity ratio was less than 1. They investigated[10] the effect of drawing on the structure and physical properties (tensile strength, elongation) of the PP/N6 polyblend fibers. Also, they examined[11] the effect of the fractions

Correspondence to: R. Kotek (rkotek@unity.ncsu.edu).

TABLE I
Compositions, Take-up Speeds, and Draw Ratios Used for Making Alloy Filaments

Sample code	PP (wt %)	N6 (wt %)	PP-*g*-MAH (wt %)	Take-up speed (m/min)	Draw ratio
A1	100	0	0	300	—
A2	90	10	0	300	—
A3	85	10	5	300	—
A4	75	20	5	300	—
A5	100	0	0	800	—
A6	90	10	0	800	—
A7	85	10	5	800	—
A8	75	20	5	800	—
A9	100	0	0	300	3.5
A10	90	10	0	300	3.5
A11	85	10	5	300	3.5
A12	75	20	5	300	3.5
A13	100	0	0	800	2
A14	90	10	0	800	2
A15	85	10	5	800	2
A16	75	20	5	800	2

of PP and N6 components on the creep characteristics of the fiber.

Grof and coworkers et al.[12] showed, by addition of the interface modifier, PP-*g*-MAH, the fiber extrusion process became more effective and the properties of the fibers (tenacity and modulus) improved. These investigators also examined the effect of drawing on the physical properties of PP/N6 fibers in which N6 fraction was varied over 0 to 10 wt %.[13,14]

Liang and coworkers[15] investigated the effect of extruding PP/N6 through a capillary rheometer on the rheology and phase morphology and also studied the development of structure during melt spinning of fibers.

As was shown in our previous paper,[31] N6 droplets coalesced during melt spinning and led to the development of fibrillar morphology in polyblend fibers. In the present study, alloy filaments were produced from PP and N6 containing 0 and 10% N6 and 0% PP-*g*-MAH in one set and 10 and 20% N6 along with 5% PP-*g*-MAH in another set. The melt spun filaments were taken up at two different speeds, namely 300 and 800 m/min. For studying the effect of drawing on orientation in the crystalline and amorphous regions of PP and N6 phases, the alloy filaments were drawn at two draw ratios, 3.5× for filaments extruded at 300 m/min and 2× for filaments extruded at 800 m/min. For calculating orientation factors in the amorphous regions of PP and N6 of the alloy filaments, two different methods involving different assumptions were used. Morphology was examined using a laser scanning confocal microscopy (LSCM). The orientation factor of crystalline regions was determined with a wide-angle X-ray diffraction (WAXD) unit. Tensile properties (tenacity, elongation at break, and modulus) were determined using standard ASTM methods. Sonic modulus was determined using a pulse propagating meter (PPM-5R). The wetting characterics, including contact angle and work of adhesion, were determined using a Wilhelmy dynamic contact angle device. A number of models were used for understanding the experimental values of tenacity and modulus found in the alloy filaments.

EXPERIMENTAL

Materials

Commercial fiber grade isotactic polypropylene known as Escorene was obtained from Exxon Chemical Co. PP had a melt flow index (MFI) of 16.7 g/10 min, density of 0.97 g/cm^3, and T_m of 170°C. Fiber grade nylon 6 was supplied by Allied Signal Co., USA. N6 had MFI of 27.6 g/10 min, density of 1.14 g/cm^3, and T_m of 220°C). PP-*g*-MAH (trade name PB 3150) was received from Uniroyal Chemical Co., USA. This polymer had MFI of 50 g/10 min, MAH index of 1.5%, and density of 0.9 g/cm^3. Table I shows the composition of filaments, take-up speeds and draw ratios.

Fiber spinning

Before melt spinning, the N6 polymer chips were dried in a vacuum oven for 24 h at 80°C. The melt spinning process was performed on the Alex James and Assoc. Inc melt extruder with a spinneret containing 64 holes, each with 0.6 mm diameter and 2.3 L/D ratio. The processing temperatures were controlled at five different zones in the extruder from the feed to die; the temperatures were 235, 245, 250, 265, and 270°C. Undrawn filaments were taken-up at 300 and 800 m/min.

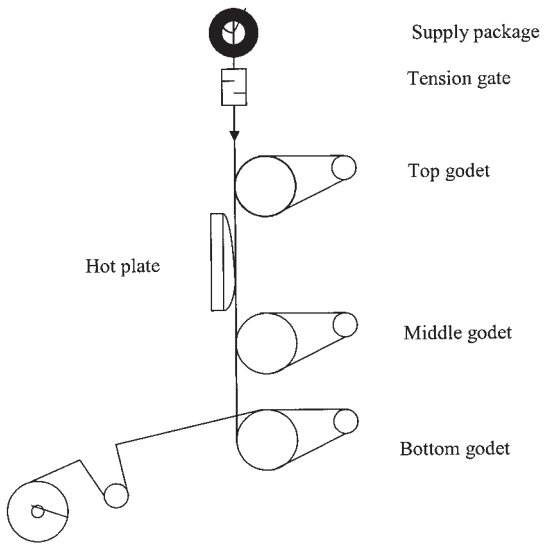

Figure 1 Arrangement of Diens drawing unit used for drawing alloy filaments.

Drawing of filaments

The filament yarns were drawn on a Dienes single-position experimental drawing unit (Dienes Apparatebew GMBH, Mulheim, Germany). Figure 1 illustrates the arrangement of the drawing rollers employed in this investigation. The temperature of hot plate was 120°C and that of the rollers was 100°C. The samples collected at 300 m/min were drawn at 3.5× and those collected at 800 m/min were drawn at 2×.

Tensile properties

Stress–strain curves of single alloy filaments were obtained using a Sintech tensile tester at 65% RH and 20°C, with a gauge length of 5 cm and a cross-head speed of 25 cm/min (ASTM D 2256).

Sonic modulus

For determining sonic modulus, a pulse propagation meter (Dynamic Modulus Tester PPM-5R, H. M. Morgan Co. Inc.) was used. This device relies on the principle of measuring the velocity of longitudinal waves through the specimen. The distance between two piezoelectric transducers, one acting as the transmitter and the other as the receiver, which are in contact with the specimen, changes during the test. The velocity of the pulse is determined by the slope of a plot of the distance against time. The sonic modulus was calculated by the following relationship reported by Moseley:[16]

$$E = 11.3 \times C^2 \quad (1)$$

where C represents the sonic velocity in Kms $^{-1}$ and E represents Young's modulus (gf/denier).

Wetting characteristics

For measuring surface wetting properties of a single filament, we used the Wilhelmy balance (Cahn C-2000).[18] The technique yields the values of the advancing and the receding contact angles by evaluating the forces that cause the liquid interline to advance or recede, respectively, over the surface of the filament. According to the Wilhelmy principle, the vertical component of the attractive force across the interface between a partially immersed solid and a liquid surface is expressed as follows:

$$F_w = \gamma_{LV} P \cos \theta \quad (2)$$

where F_w is the wetting force (dyne), γ_{LV} is the surface tension of the liquid (dyne/cm), P is the perimeter of the fiber (cm), and θ is the contact angle between the liquid and fiber surface.

The term $\gamma_{LV} \cos \theta$ can also be used to define a parameter called the wettability index (WI), which gives a normalized or intrinsic value of the Wilhelmy force, i.e.:

$$WI = \frac{F_W}{P} = \gamma_{LV} \cos \theta \quad (3)$$

Using the procedure described elsewhere,[18] a specimen was prepared in which the end was loaded with a platinum sinker and the assembly was suspended from the balance and tared and was traversed into and out of the liquid (deionized ultrafiltered water) at 750 μm/min. From the sum of the measured force and the calculated buoyancy force of the sinker, the value of the Wilhelmy force was calculated. This, divided by the product of the perimeter of the fiber and the surface tension of the fluid, gave the value of the cosine of the contact angle. For each specimen, three determinations were made for both the advancing and the receding modes.

Laser scanning confocal microscopy

LSCM is nondestructive powerful tool for examining and reconstructing the underlying (embedded) three-dimensional structures with a high degree of accuracy.[18] The added advantage of using this technique on two-phase polymeric material is that the light beam interacts with each of the phases differently. This allows an effective means for examining and characterizing *in situ* the phase distribution and separation phenomena in polyblend materials.[18] The microscope can be used to construct images in various scanning

modes, including planar (*XY* scan), vertical (*XZ* scan), and time-dependent programmed mode. Only limited work involving the use of LSCM of fiber has appeared in scientific literature. To our knowledge, morphology of alloy filaments has not been studied using this technique.

The fibers were imaged using Leica DMRBE LSCM, which was equipped with three laser systems: an Ar-ion (488 and 514 nm), a Kr-ion (568 nm), and a He-Ne (632.8 nm). For the purpose of imaging, the 488 nm line of the Ar-ion laser was used in conjunction with a 40× NA 1.25 oil immersion objective.

X-ray analysis of polyblend fibers

A Siemens X-ray diffraction unit, operated at 30 KV and 20 mA, with a Cu Kα (λ = 1.54 Å) line, was used to estimate the crystal size and the magnitude of the crystalline orientation. The alloy filaments were hand wound parallel on a sample holder; the latter was positioned perpendicular to the axis of X-ray beam.

The 040 and 110 monoclinic reflections of PP were recorded and used to compute Hermans–Stein crystalline orientation factors.[19] These factors can be used to indicate the orientation of the third crystallographic axis with respect to the fiber axis. They are defined in such a way that the orientation factor is unity if the crystallographic axis is aligned parallel to the fiber axis, −0.5 if the axis is aligned perpendicular to the fiber axis, and 0 if the axis is distributed randomly in the sample. The orientation factor is given by

$$f_j = (3\cos^2\phi_{j,z} - 1)/2 \tag{4}$$

where $\cos^2\phi_{j,z}$ is the average value of the square of the cosine of the angle between the fiber axis and the j crystallographic axis (j = a, b, or c). Assuming rotational symmetry about the fiber axis, the value of this quantity is given as follows:

$$\cos^2\phi_{j,z} = \frac{\int_0^{\pi/2} I_{hkl}(\phi_{j,z})\cos^2\phi_{j,z}\sin\phi_{j,z}d\phi_{j,z}}{\int_0^{\pi/2} I_{hkl}(\phi_{j,z})\sin\phi_{j,z}d\phi_{j,z}} \tag{5}$$

where $I_{hkl}(\phi_{j,z})$ is the intensity of the diffracted beam from the (hkl) planes that are normal to the j-crystallographic axis.

Using eqs. (4) and (5), the value of f_b was computed from the intensity distribution in the 040 reflection. In monoclinic polypropylenes, the chains are helically configured whose axes lie along the c-crystallographic axis. In oriented fibers there is no convenient set of diffraction planes that lie perpendicular to the c-axis, and, therefore, the method of Wilchinsky[20] was used to compute f_c. Wilchinsky[20] has shown that, for monoclinic polypropylene,

$$\cos^2\phi_{c,z} = 1 - 1.1099\cos^2\phi_{110,z} - 0.901\cos^2\phi_{040,z} \tag{6}$$

where $\cos^2\phi_{110,z}$ and $\cos^2\phi_{040,z}$ are obtained from intensity measurements on the 110 and 040 reflections. Therefore, the quantity $\cos^2\phi_{c,z}$ was determined using eq. (6).

Crystal size was calculated from the Scherrer's equation:[21]

$$L = \frac{0.9\lambda}{\beta\cos\theta} \tag{7}$$

where L is the crystallite dimension, λ is the wavelength, and β is the breadth at half maximum intensity.

For orientation of the pseudohexagonal nylon 6[15] in melt spun fibers, we used the 002 equatorial reflection.

$$\cos^2\phi_{c,z} = 1 - 2\cos^2\phi_{002,z} \tag{8}$$

$$f_a = f_b = -f_c/2 \tag{9}$$

Birefringence measurements

Birefringence was measured with an interference microscope (Martin Microscope Co). The objective lens used was 12.5×, 0.25 NA. The magnitude of amorphous orientation in the fibers was determined using the theory of Stein and Norris.[20] The total birefringence is composed of the amorphous and the crystalline contributions and of the form value:

$$\Delta n = f_c x\Delta n_c^\circ + f_{am}(1-x)\Delta n_{am}^\circ + \Delta n_{form} \tag{10}$$

where Δn_c° and Δn_{am}° are the intrinsic birefringences of the crystalline and amorphous regions, respectively, and x is the degree of crystallinity. For intrinsic values of birefringence of PP, we accepted the results of Samuels, i.e., Δn_c° = 0.0331 and Δn_{am}° = 0.0468,[22] and for N6 we accepted the values calculated by Balcerzyk et al.,[23] Δn_c° = 0.089 and Δn_{am}° = 0.078. Δn_{form} is the so-called form birefringence[24] and was calculated from eq. (11):

$$\Delta n_{form} = \frac{\phi_1\phi_2(n_1^2 - n_2^2)}{2n_{11}[(\phi_1+1)n_2^2 + \phi_2 n_1^2]} \tag{11}$$

where ϕ_1 and ϕ_2 are the volume fractions of the dispersed phase (Nylon 6) and the matrix (PP), respectively, and n_1 and n_2 are their corresponding refractive indices. n_{11} refers to the refractive index of the blend composition along the fiber axis.

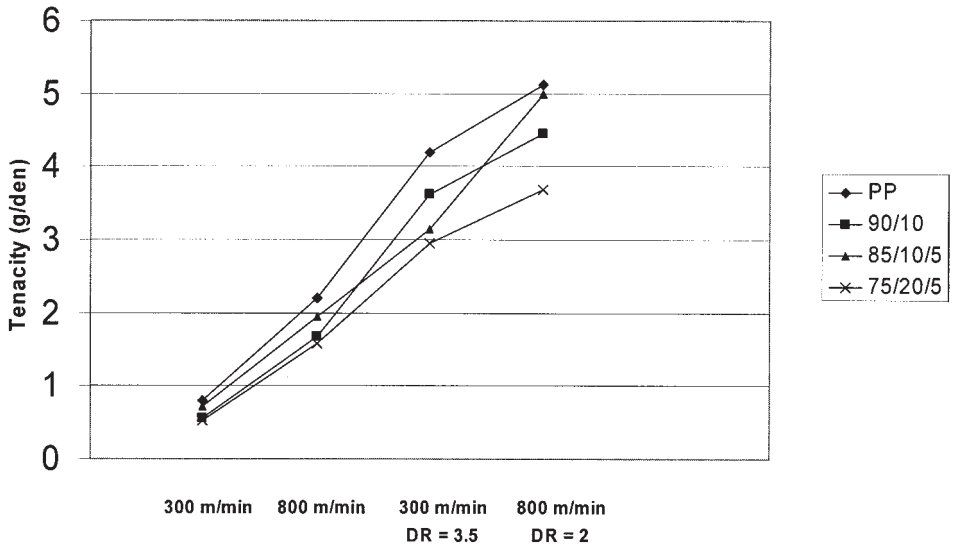

Figure 2 Tenacity (g/denier) of undrawn and drawn PP and alloy filaments.

Calculations for the alloy filaments show that Δn_{form} is about 0.0005 for (90/10), 0.00048 for (85/10/5), and 0.000848 for (75/20/5) compositions. Accordingly, the form birefringence had little contribution to the total birefringence and was therefore neglected in the calculations. To calculate f_{am}, we used Δn from birefringence measurements, x from DSC, and f_c from WXRD measurements.

Thermal properties

A Perkin–Elmer differential scanning colorimeter (Model DSC7), calibrated with indium, was used to study the thermal behavior of the alloy filaments. Specimens of 3 to 5 mg were encapsulated in aluminum pans and heated at the rate of 20°C/min from the room temperature to 250°C and subsequently cooled to the room temperature. The fusion enthalpies, $\Delta H_{f,PP}$ and $\Delta H_{f,N6}$, were measured and the degrees of crystallinity, $\chi_{c,PP}$ and $\chi_{c,N6}$, were calculated from the following equations:

$$\chi_{c,N6} = \frac{\Delta H_{f,N6}}{\Delta H^{\circ}_{f,N6}} \times \frac{1}{w_{N6}} \times 100 \quad (12)$$

$$\chi_{c,PP} = \frac{\Delta H_{f,PP}}{\Delta H^{\circ}_{f,PP}} \times \frac{1}{w_{PP}} \times 100 \quad (13)$$

where $\Delta H^{\circ}_{f,PP}$ and $\Delta H^{\circ}_{f,N6}$ are the fusion enthalpies of completely crystalline PP and N6 materials,[26] respectively, and w_{PP} and w_{N6} are the corresponding weight fractions of the two materials in the alloy filaments. The values of ΔH°_f were taken from the literature, which were 50 and 55 cal/g, respectively, for PP and N6.[26]

RESULTS AND DISCUSSION

Figures 2–4 show that, with increasing take-up speed and draw ratio, the values of tenacity and modulus increased and that of elongation at break (%) decreased for all filaments. Lower values of mechanical properties of the alloy filaments compared to those of the neat PP material is due to the presence of cracks or microvoids (flaws) at the interface of the alloy filaments that lead to concentration of stresses.[14] The alloy filaments, however, clearly have adequate tensile strength for most practical uses.

The figures show that, with increasing amounts of N6, tenacity, modulus, and elongation (%) at break decreased. The alloy filaments containing 10 wt % of N6 generally show higher values of tenacity, modulus, and elongation (%) at break with the compatibilizer than without it. This is most likely due to relatively greater adhesion between PP and N6 in the presence of PP-*g*-MAH. Similar results have been reported on the effect of compatibilizer on modulus by Grof et al.[12] and on tenacity and elongation by Takahashi et al.[10] in PP/N6 polyblend fibers.

The stress–strain curves of alloy filaments show brittle behavior (Fig. 5) while those of PP filaments (Fig. 6) show ductile behavior. This change is particularly observed in transition from PP (100/0/0) to the alloy (75/20/5) filaments. Lower values of tensile properties noted above in the alloy filaments support the presence of brittle character. The latter is considered to be due to the existence of cracks or voids (flaws) in the matrix (PP) that act as stress concentration points.

Several investigators have proposed models for estimating the values of tensile properties of alloy filaments; among these are Leidner[26] and Nielsen[27,28] for

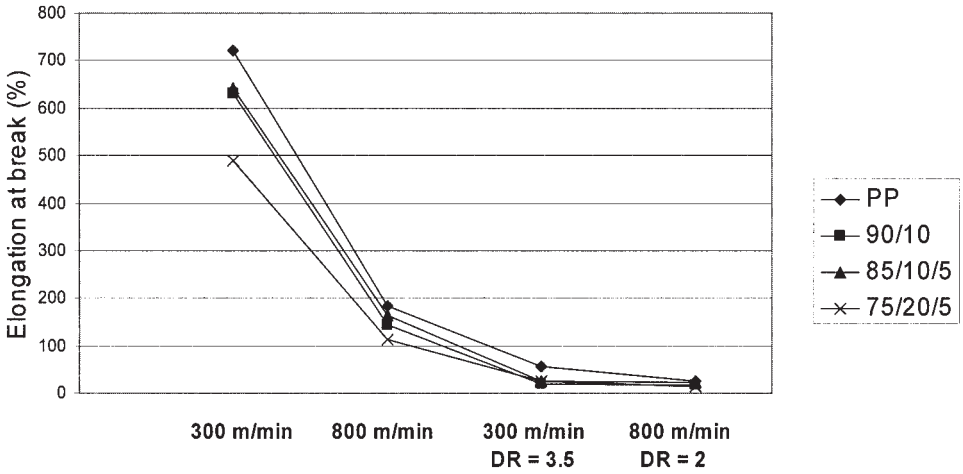

Figure 3 Elongation at break (%) of undrawn and drawn PP and alloy filaments.

tenacity and Paul[29] for elastic modulus. We used these models for calculating the values of tenacity and modulus for our materials.

Leidner model

The Leidner equation[26] applies to the case of no adhesion between the matrix and the inclusion, so that the stress is transferred from the matrix to the spherical inclusion by frictional forces only. In this model the tenacity is given by

$$\sigma = \sigma_m(1 - \phi_2) \tag{14}$$

where ϕ_2 is the volume fraction of N6 and σ_m is the tenacity of matrix (PP).

Leidner equation could be fitted to the experimental data by a linear regression with a correlation coefficient $r^2 = 0.97$.

Nielsen model

Nielsen[27] also proposed a tenacity equation for a blend system having spherical inclusions and no adhesion between the matrix and the inclusions:

$$\sigma = \sigma_m(1 - \phi_2^{2/3})S \tag{15}$$

where, S is the stress concentration function, which has a value of 1 (maximum) when there is no stress concentration. The values of tensile strength calculated by this model assuming $S = 1$ may be considered as maximum, since stress concentrations will tend to

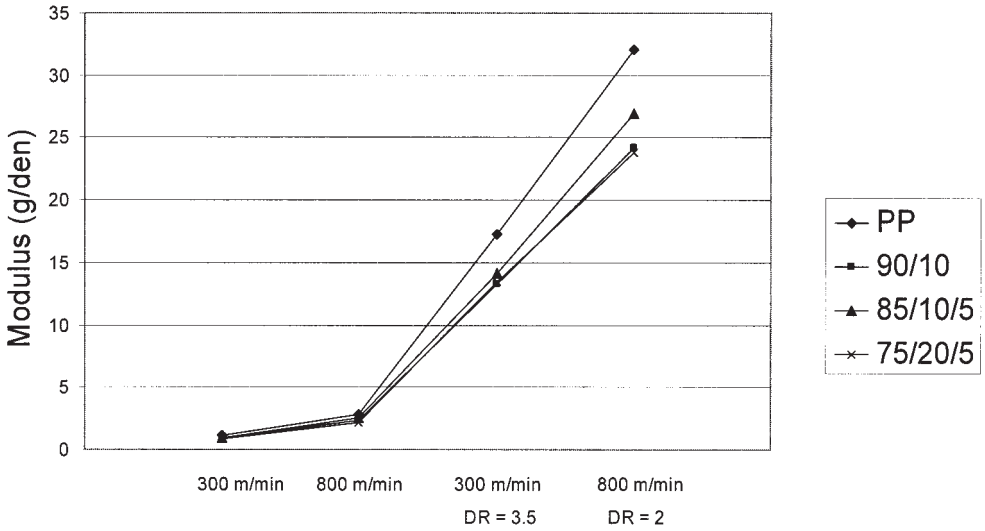

Figure 4 Modulus of undrawn and drawn PP and alloy filaments.

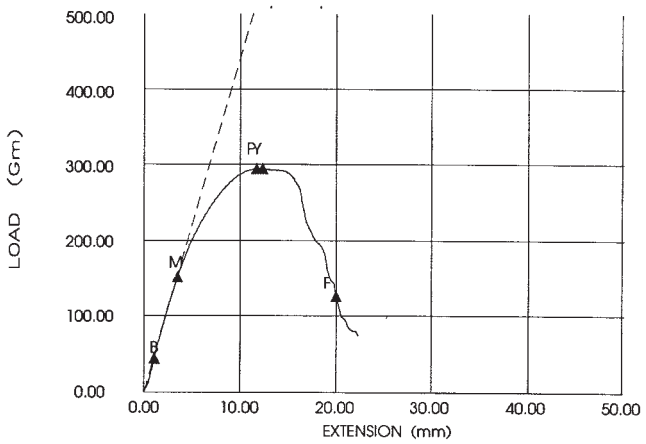

Figure 5 Stress–strain curve of (75/20/5) alloy filament produced at take-up speed of 300 m/min and draw ratio of 3.5.

lower the values. We calculated the tenacity with this model and used linear regression to correlate the calculated values with the experimental and obtained the following results: $S = 0.5$ ($r^2 = 0.647$), 0.6 ($r^2 = 0.75$), 0.7 ($r^2 = 0.839$), 0.8 ($r^2 = 0.908$), 0.9 ($r^2 = 0.954$), and 1 ($r^2 = 0.978$).

Modified Nielsen model

Nielsen[28] suggested that eq. (16) must be used for tensile strength when voids or holes are present in the system.

$$\sigma = \sigma_m \exp(-a\phi_2) \tag{16}$$

with a proper choice of the value of the constant a, a theoretical fit for the experimental values can be obtained. The negative sign comes from the assumption that the property decreases with an increase in the volume fraction of the holes. When hard inclusions are present in the matrix, a positive sign can be used for the property increase. We calculated tenacity with this model for different values of the constant a and, as before, correlated these with all the values found experimentally, with the following results: $a = 0.5$ ($r^2 = 0.956$), 0.6 ($r^2 = 0.96$), 0.7 ($r^2 = 0.964$), 0.8 ($r^2 = 0.967$), 0.9 ($r^2 = 0.97$), and 1 ($r^2 = 0.973$).

Paul's model

For examining the relationship between composition and interfacial adhesion and modulus, we used Paul's equation.[30] Paul used the energy theorems of elasticity theory and derived the solution for the elastic modulus in tension for two phase materials, the assumption being that both matrix (m) and inclusion (i) have the same value of Poisson's ratio. For the system having perfect adhesion at the boundary:

$$E = E_m \frac{E_m + (E_i - E_m)\phi_2^{2/3}}{E_m + (E_i - E_m)\phi_2^{2/3}(1 - \phi_2^{1/3})} \tag{17}$$

For the system in which the particle inclusions are loose:

$$E = E_m \frac{(1 - \phi_2^{2/3})}{1 - \phi_2^{2/3}(1 - \phi_2^{1/3})} \tag{18}$$

We used eq. (18) and found correlation with the experimental data given by $r^2 = 0.967$. The effect of interfacial adhesion has not been considered in any of these equations and, therefore, we could not account for the effect of compatibilizer on the properties by any of these models.

Figure 7 shows that sonic modulus of all filaments increased with an increase in the take-up speed and draw ratio. The undrawn and drawn alloy filaments show higher values of sonic modulus than do the PP filaments. The sonic modulus values of drawn alloy filaments with 10 wt % or more N6 are higher with compatibilizer than without it. Increasing interfacial adhesion between PP and N6 by adding compatibilizer obviously increased the velocity of propagation of sonic pulse. An increase in sonic modulus with the amount of N6 shows that, at such high frequency, N6 starts to take up the force and contribute to the properties. But under static conditions (Instron tests) this does not happen and, therefore, the Instron modulus of the alloy filaments is lower than that of the neat PP filaments. A higher value of the sonic modulus than the static is obviously due to the former being more nearly the elastic modulus while the latter is the so called complex modulus, governed by both the elastic or storage and the viscous or loss effects.

Percent crystallinity for PP and N6 components were calculated using DSC. The results, given in Table II, show that, with an increase in take-up speed and

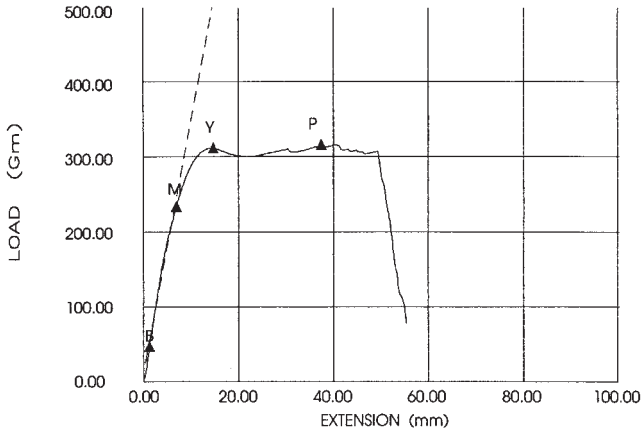

Figure 6 Stress–strain curve of PP filaments produced at take-up speed of 300 m/min and draw ratio of 3.5.

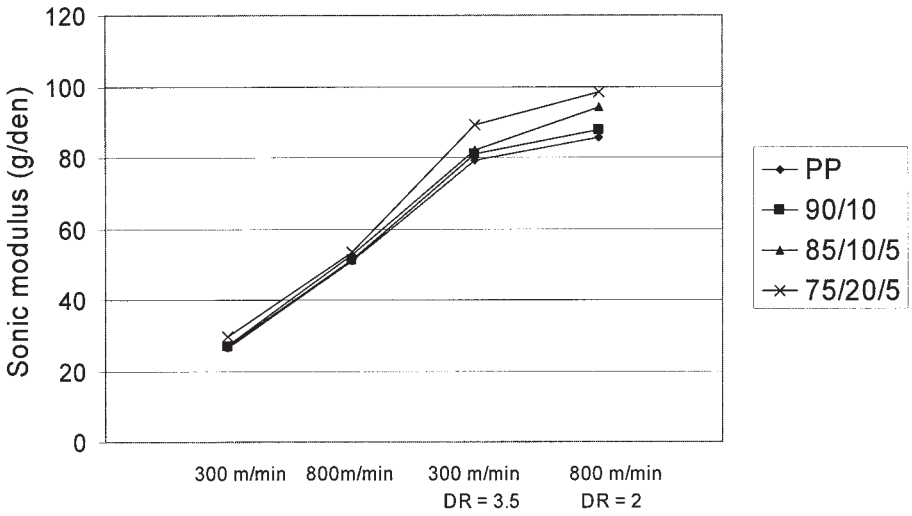

Figure 7 Sonic modulus of undrawn and drawn PP and alloy filaments.

draw ratio, the percent crystallinity of PP and N6 components in the alloy filaments increased.

Also, as shown in this table, the total birefringence increased with an increase in the fraction of N6, the take-up speed, and the draw ratio.

Calculation of the amorphous orientation factor

Orientation factor for the crystalline region was calculated from the X-ray diffraction data. The results showed that, with an increase in the amount of N6, the orientation factor for the crystalline region decreased for PP, but increased for N6. The orientation factor for the crystalline regions of PP and N6 in alloy filaments is slightly higher with compatibilizer than without it.

For calculating the orientation factor for amorphous regions in the alloy material, we used values of birefringence from optical microscopy, percent crystallinity from DSC data, and f_c for PP and N6 from the X-ray data.

We assumed that the following relations should hold in the alloy filaments:

$$\Delta n_c^\circ = w_{pp} \times \Delta n_{c,pp}^\circ + w_{N6} \times \Delta n_{c,N6}^\circ \quad (19)$$

$$\Delta n_{am}^\circ = w_{pp} \times \Delta n_{am,pp}^\circ + w_{N6} \times \Delta n_{am,N6}^\circ \quad (20)$$

TABLE II
Crystallinity, Orientation Factor of Crystalline Regions, Crystal Size, and Birefringence of Alloy Filaments Produced with Various Speeds and Draw Ratios

Sample code PP/N6/PP-*g*-MAH	% Crystallinity of PP	% Crystallinity of N6	$f_{c,PP}$	$f_{c,N6}$	L (Å)	Δn
300 m/min						
A1 (PP)	38.8	—	0.16	—	18.73	0.00641
A2 (90/10/0)	33.45	14.1	0.13	0.003	37.21	0.00643
A3 (85/10/5)	42.67	9.38	0.136	0.007	24.83	0.00658
A4 (75/20/5)	53.82	10.85	0.096	0.035	28.39	0.00985
800 m/min						
A5 (PP)	45.52	—	0.40	—	25.09	0.01747
A6 (90/10)	40.32	18.9	0.35	0.12	31.72	0.018683
A7 (85/10/5)	43.1	14.3	0.38	0.14	43.55	0.019023
A8 (75/20/5)	53.7	25.8	0.34	0.18	70.8	0.02063
300 m/min, DR = 3.5						
A9 (PP)	46.52	—	0.58	—	47.94	0.028683
A10 (90/10)	47.64	26.0	0.54	0.16	51.5	0.029135
A11 (85/10/5)	50.28	25.72	0.55	0.17	60.24	0.030381
A12 (75/20/5)	63.21	29.7	0.44	0.21	72.3	0.031649
800 m/min, DR = 2.0						
A13 (PP)	44.9	—	0.73	—	48.9	0.031472
A14 (90/10)	49.12	21.02	0.68	0.31	51	0.031968
A15 (85/10/5)	51.01	15.3	0.71	0.32	50.4	0.032431
A16 (75/20/5)	68.61	38.1	0.64	0.36	68.32	0.034215

TABLE III
Orientation Factor of Amorphous Regions Calculated by Different Methods

Sample code PP/N6/PP-*g*-MAH	$\bar{f}_{am}$	$f_{am,PP}$	$f_{am,N6}$
300 m/min			
A1 (PP)	0.152	0.152	—
A2 (90/10)	0.146	0.064	0.044
A3 (85/10/5)	0.166	0.062	0.042
A4 (75/20/5)	0.289	0.099	0.082
800 m/min			
A5 (PP)	0.449	0.449	—
A6 (90/10)	0.446	0.394	0.016
A7 (85/10/5)	0.484	0.398	0.018
A8 (75/20/5)	0.542	0.396	0.032
300 m/min, DR = 3.5			
A9 (PP)	0.789	0.789	—
A10 (90/10)	0.746	0.617	0.0311
A11 (85/10/5)	0.855	0.676	0.0278
A12 (75/20/5)	0.982	0.667	0.0994
800 m/min, DR = 2.0			
A13 (PP)	0.799	0.800	—
A14 (90/10)	0.762	0.647	−0.0049
A15 (85/10/5)	0.833	0.652	0.0172
A16 (75/20/5)	0.979	0.591	−0.0250

$$f_c = w_{PP} \times f_{c,PP} + w_{N6} \times f_{c,N6} \tag{21}$$

$$\chi_c = w_{PP} \times \chi_{c,PP} + w_{N6} \times \chi_{c,N6} \tag{22}$$

$$\Delta n_{alloy} = \chi_c f_c \Delta n_c^\circ + (1 - \chi_c)\bar{f}_{am}\Delta n_{am}^\circ \tag{23}$$

where w, x, and f are weight fraction, fractional crystallinity, and orientation factor, respectively. Δn_c° and Δn_{am}° are the intrinsic birefringences of the crystalline and the amorphous regions, respectively. In this method, we calculated the average value of the orientation factor for the amorphous regions of alloy filaments ($\bar{f}_{am}$).

With the increase in the amount of N6, the orientation factor for crystalline regions of PP decreased and that of N6 increased in both the undrawn and the drawn alloy filaments (Table II). Liang and coworkers[15] had shown that, for a given spinline stress, with increase in the fraction of N6, the orientation factor of crystalline region decreased for PP but increased for N6; this agrees with the results we obtained. The crystal size of plane (110) of PP increased with increase in the take-up speed and the draw ratio. Teli and coworkers[30] reported an increase of crystal size of PP for plane (110) in fibers from blend of PP/PBT and PP/PET. It is clear from the results of crystallite size based on the (110) plane of PP that in alloy filaments crystals grow in size with an increase in the amount of N6. Such an increase in the size of the crystals seems to bring down the orientation of chain molecules in PP crystals.

As noted from the results in Table III, with an increase in the amount of N6 the orientation factor of amorphous regions in the compatibilized PP/N6 alloy filaments $\bar{f}_{am}$ increased. An increase in the take-up speed and draw ratio also led to significant increase in the orientation factor for amorphous regions. It is interesting to note that the amorphous orientation factor $\bar{f}_{am}$ is quite high (> 0.7) for materials that were drawn and, in two instances (75/20/5), the value approached unity, which is expected of a perfectly oriented structure.

Next, we estimated the values of f_{am} for two components. For this, we assumed that the birefringence of the neat N6 was 0.03 for undrawn and 0.055 for drawn filaments. These values were taken from the information in the literature.[23] Additionally, it was considered that the contributions by Δn of PP and N6 to that of the alloy filament depended on the mass fractions of PP and N6. We assumed that the mass fraction of PP included the mass fraction of the compatibilizer in the material. Using this concept [eq. (24)], we calculated birefringence of PP and then orientation factors for the amorphous areas of PP and N6 from eqs. (25) and (26).

$$\Delta n_{alloy} = w_{PP}\Delta n_{PP} + w_{N6} \times \Delta n_{N6} \tag{24}$$

$$w_{PP}\Delta n_{PP} = \chi_{c,PP} f_{c,PP}\Delta n_{c,PP}^\circ + (1 - \chi_{c,PP}) f_{am,PP}\Delta n_{am,PP}^\circ \tag{25}$$

$$w_{N6}\Delta n_{N6} = \chi_{c,N6} f_{c,N6}\Delta n_{c,N6}^\circ + (1 - \chi_{c,N6}) f_{am,N6}\Delta n_{am,N6}^\circ \tag{26}$$

Saito and Innoue[32] used a similar approach [eq. (27)] to estimate the composition of miscible polymers where positive and negative birefringences cancel out and result in a birefringence-free mixture.

$$\Delta n = \Delta n_A^\circ f_A \phi_A + \Delta_B^\circ f_B \phi_B + \Delta n_F \tag{27}$$

where Δn_i° is the intrinsic birefringence of i polymer, f_i is the orientation factor, ϕ_i is the volume fraction, and Δn_F is the form birefringence, which is assumed to be zero for the miscible blends.

The results from this method for the noncompatible pair of polymers, namely polypropylene and nylon 6, show that, with an increase in the fraction of N6, $f_{am,PP}$ generally varied but was lower than that for the corresponding PP filament. Since the orientation factors for the crystalline and amorphous regions of N6 are generally very low, the values of $\bar{f}_{am}$ [eq. (23)] and $f_{am,PP}$ are reasonably close. Accordingly, most of the force generated in drawing or spinning is borne by PP, which implies that the behavior of the alloy filaments of this study is similar to those of the isostrain systems.

Fiber morphology determined with laser scanning confocal microscopy

LSCM micrographs of the structure of the alloy filaments are included in Figures 8–11. The photographs

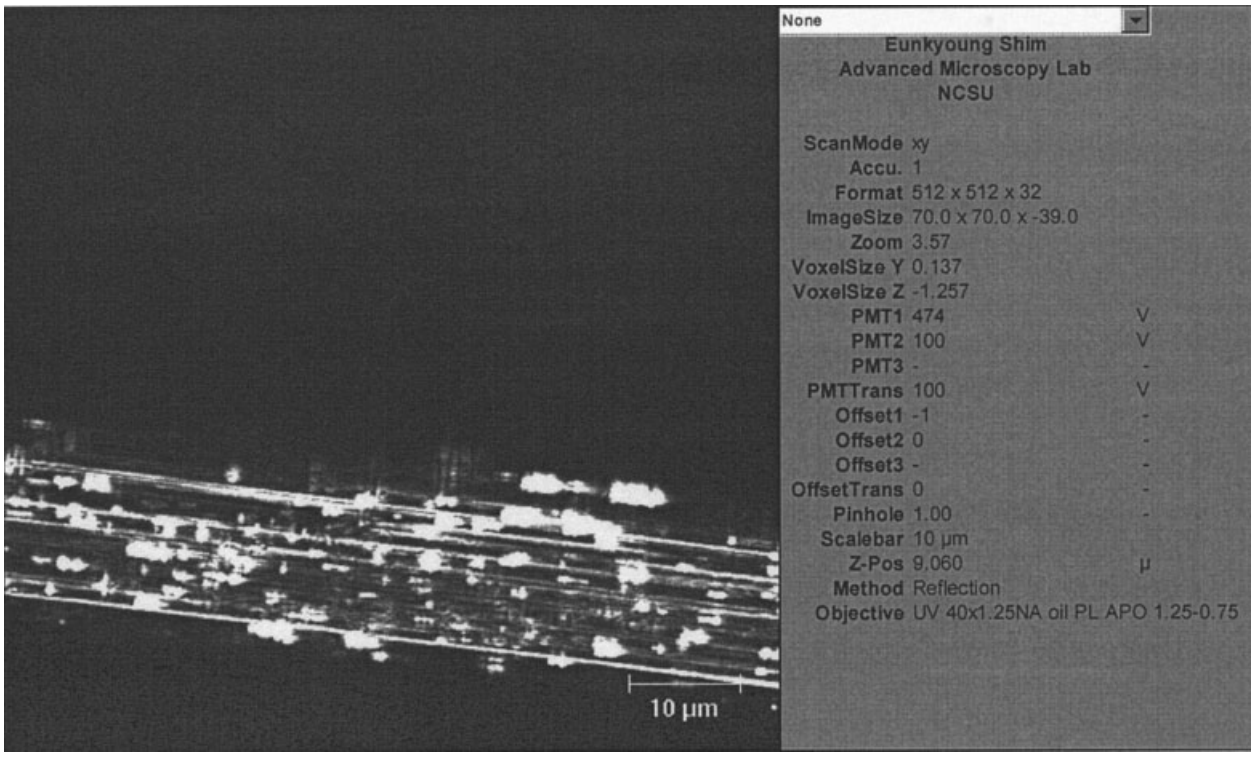

Figure 8 LSCM micrograph of (90/10) PP/N6 alloy filament at take-up speed of 800 m/min.

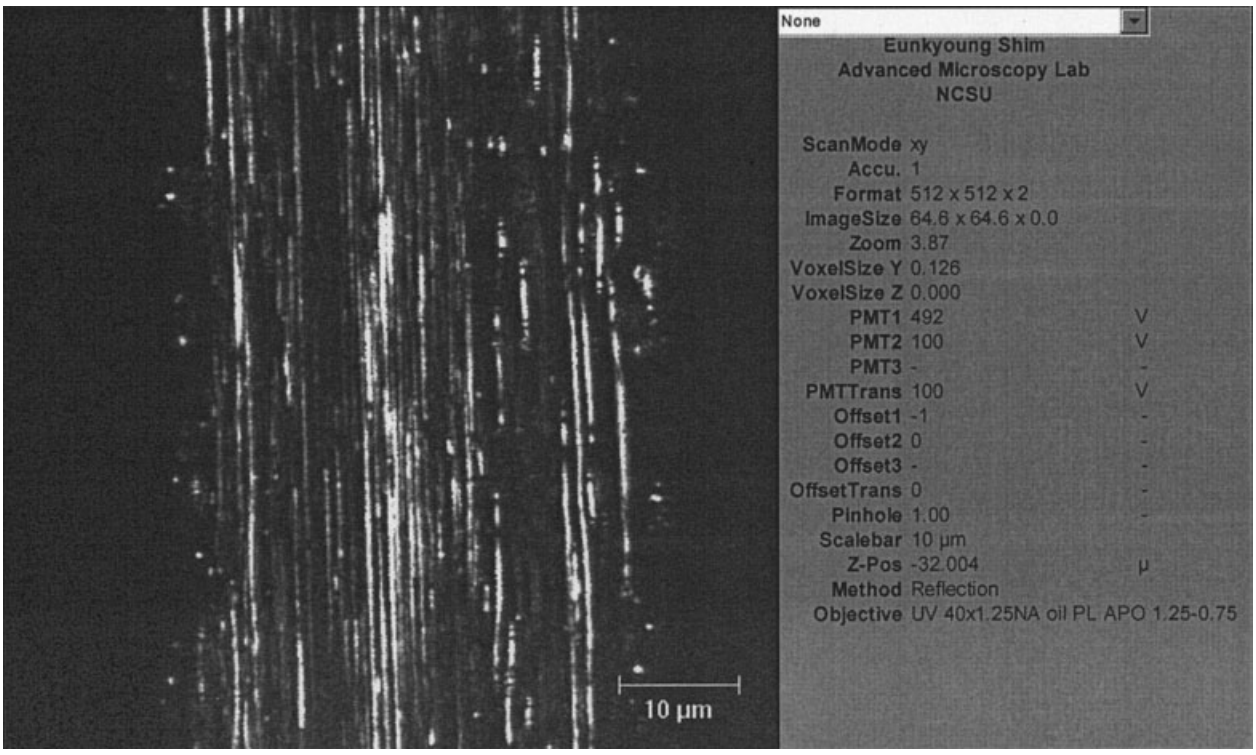

Figure 9 LSCM micrograph of (85/10/5) PP/N6/PP-*g*-MAH alloy filament at take-up speed 300 m/min.

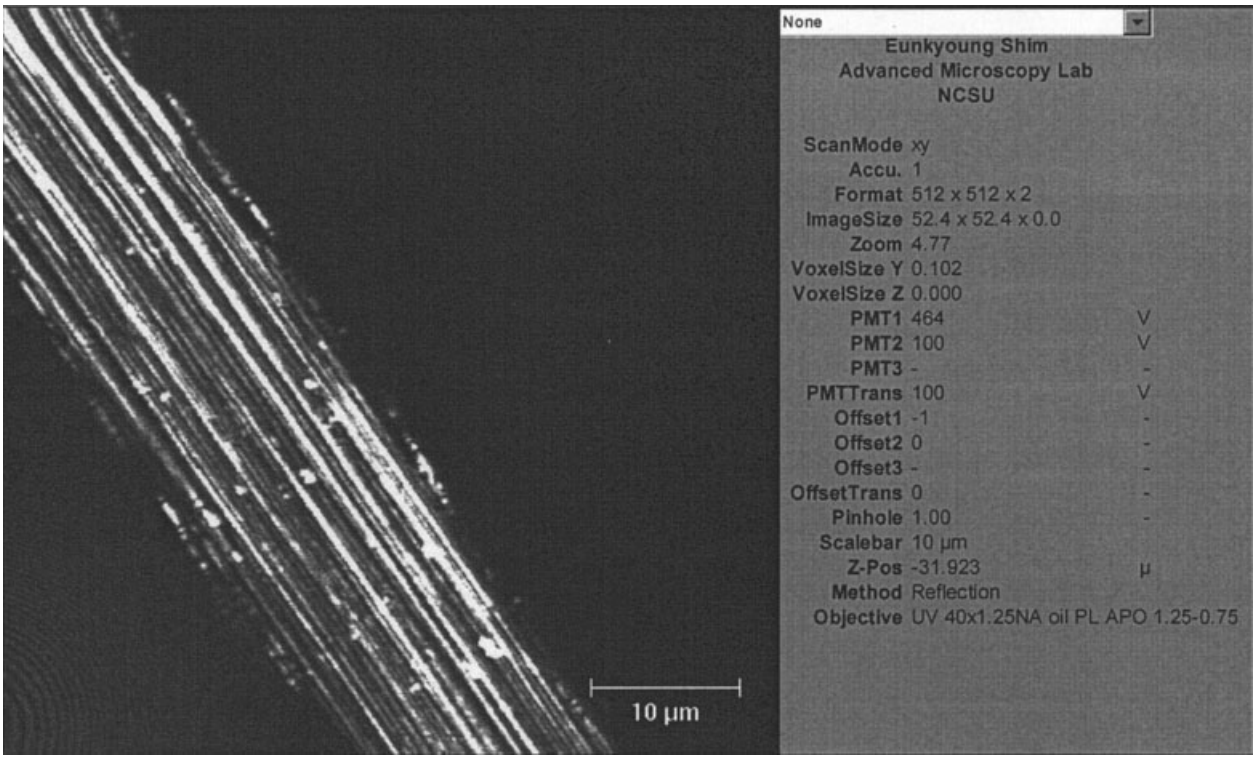

Figure 10 LSCM micrograph of (85/10/5) PP/N6/PP-*g*-MAH alloy filament at take-up speed 800 m/min.

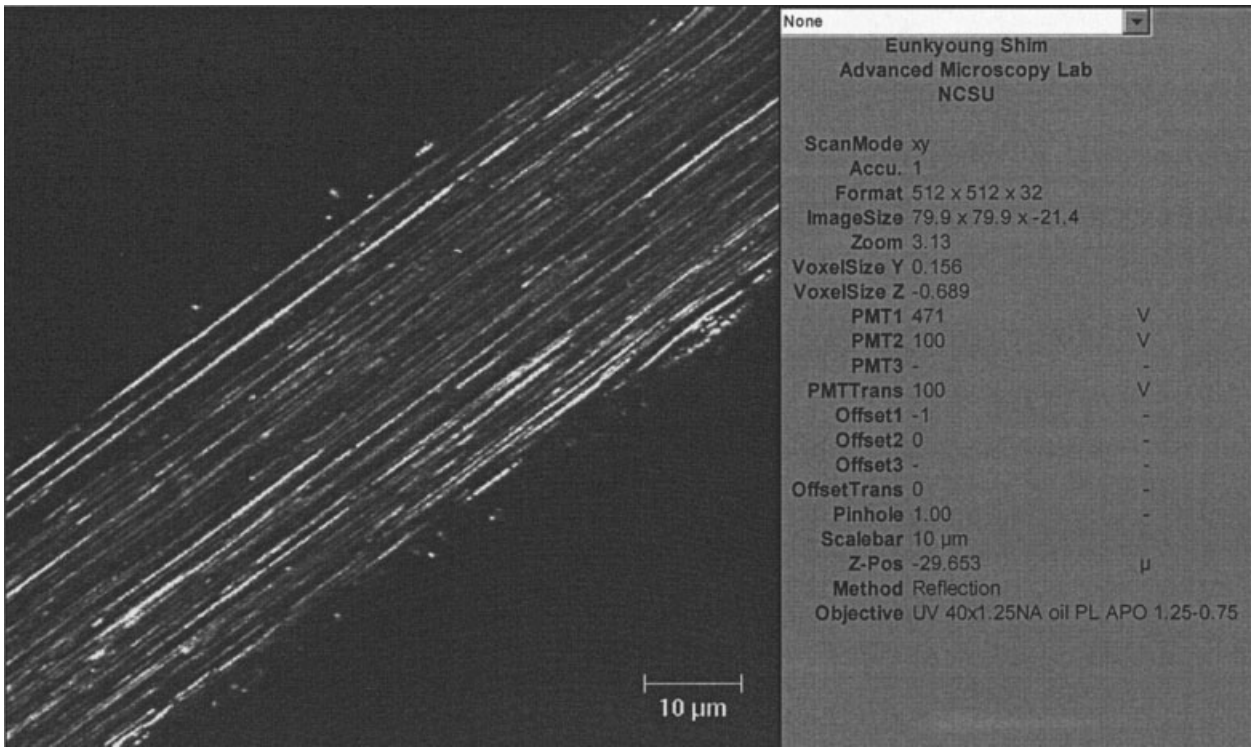

Figure 11 LSCM micrograph of (75/20/5) PP/N6/PP-*g*-MAH alloy filament at take-up speed of 300 m/min and draw ratio of 3.5.

TABLE IV
Contact Angle and Wettability Index of PP and Alloy Filaments Produced with Take-up Speed of 800 m/min

Sample code PP/N6/PP-*g*-MAH	F_a (dyne)	F_r (dyne)	θ_a (°)	θ_r (°)	WI_a	WI_r
A5 (PP)	−2.228	−1.9804	93.61	92.23	−4.58	−2.83
A6 (90/10)	−2.1599	−1.928	93.23	91.94	−4.1	−2.46
A7 (85/10/5)	−2.1293	−1.8925	93.06	91.74	−3.88	−2.21
A9 (75/20/5)	−2.0917	−1.8243	92.85	91.36	−3.27	−1.73

show matrix–fibrillar morphology with the fibrils oriented along the axis. With an increase in take-up speed and drawing, the length of fibrils seemed to increase. Variation in length of fibrils is high. The LSCM micrographs show that, in alloy filaments without the PP-*g*-MAH compatibilizer, the tendency of the fibrils to form is weak.

Wettability

Table IV shows that, with an increase in the fraction of N6, the contact angle decreased and the wettability index increased. This is expected because N6 is a more hydrophilic material than PP. Although the changes are small they are consistent. Relatively smaller changes than expected may have arisen from the fact that the disperse (N6) phase tended to largely reside in the core. This is evident from the morphology seen in Figures 8–11 wherein the boundaries of fibers lie in regions outside the fibrils.

CONCLUSIONS

We have investigated the effects of the composition and the interfacial adhesion, provided by a compatibilizer, on a number of mechanical and structural properties of PP/N6 alloy filaments made by melt spinning. Such information is valuable since polymers are being increasingly blended to produce shaped products with the goal of obtaining properties not available in neat materials. The properties considered were the tenacity, elongation at break, and the tensile and sonic moduli, among the mechanical, and the degree of crystallinity and the crystalline and amorphous orientations, among the structural. With an increase in interfacial adhesion with compatibilizer between the PP and N6 phases, tenacity, modulus, and elongation at break increased. Alloy filaments showed a relatively brittle behavior in that they had lower tensile values than did the neat PP. It is suggested that the change of the stress–strain curve from ductile for PP to brittle for alloy filaments was due to the presence of voids in the latter. The microvoids are present at the interface of PP and N6, perhaps in this polymer before it is stretched. During tensile testing, however, due to low adhesion between the two polymers, probably PP and N6 debonded and most of the force was then borne by the PP matrix. The modified Nielsen model, applicable to systems incorporating voids, showed excellent correlations with the experimental values of tenacity. Paul's model also gave good fit with the experimental values of modulus of the alloy filaments. However, these models did not account for the effect of the compatibilizer on the mechanical properties of the alloy fibers and, thus, further modeling work was necessary for such systems. Classical methods were used for estimating the values of the amorphous orientation factors for PP and N6. The assumption used was that the contributions of PP and N6 on birefringence of alloy depended on the weight fractions of the two components. With an increase in the fraction of N6 in the filaments, the crystalline orientation (f_c) decreased for PP but increased for N6. Both of these orientations increased with spinning speed and draw ratio, as expected. Likewise (110) crystal size of PP phase increased with the increase in N6 fraction, spinning speed, and draw ratio. The effect of the presence of N6 on the amorphous orientation of PP ($f_{am,PP}$) was different than noted above for $f_{c,PP}$. The values for $f_{am,PP}$ generally varied with the increase in fraction of N6 but were lower than those for the corresponding PP filaments. The value of $f_{am,N6}$ of N6 was itself very small. Accordingly the amorphous orientation of alloy, i.e., $\bar{f}_{am}$ was mostly made up of the orientation of the PP molecules. Clearly, thus, except for a negative change noted in the crystalline orientation of PP phase (Table II), all other changes in molecular structure resulting from incorporation of N6 molecules were positive. These included changes in the overall birefringence, Δn, the amorphous orientation, $\bar{f}_{am}$, the % crystallinity, and the size of PP crystals. All structural factors were enhanced with increases in spinning speed and draw ratio.

LSCM micrographs of alloy filaments showed that N6 was largely in the core and was in the form of fibrils. Fibril formation was enhanced by the presence of compatibilizer.

We thank Dr. H. Davis for useful suggestions. Richard Kotek thanks Mr. John Wefer of Uniroyal Chemical Co. for providing a gift of PB 3150.

References

1. Xanthos, M. Polym Eng Sci 1988, 28, 1392.
2. Utracki, L. A. Commercial Polymer Blends. Chapman & Hall: London, 1998.
3. Hersh, S. J Appl Polym Sci Appl Polym Symp 1977, 31, 37.
4. Heikens, D.; Barentsen, W. Polymer 1977, 18, 69.
5. Tsebrenko, M. V.; Yudin, A. V.; Ablazova, T. I.; Vinogradov, G. V. Polymer 1976, 17, 831.
6. Paul, D. R.; Newman, S. Polymer Blends, Vol. 2; Academic Press: New York, 1978.
7. Park, S. J.; Kim, B. K.; Jeong, H. M. Int Polym J 1990, 26, 131.
8. Li, X.; Chen, M.; Huang, Y. Polym J 1997, 29, 975.
9. Takahashi, T.; Konda, A.; Shimizu, Y. Sen-i-Gakkaishi 1996, 52, 507.
10. Takahashi, T.; Konda, A.; Shimizu, Y. Sen-i-Gakkaishi 1996, 52, 396.
11. Takahashi, T.; Konda, A.; Shimizu, Y. Sen-i-Gakkaishi 1996, 50, 241.
12. Grof, I.; Sain, M. M.; Durcova, O. J Appl Polym Sci 1992, 44, 1061.
13. Grof, I.; Durcova, O.; Marcincin, A. Acta Polym 1989, 40, 344.
14. Grof, I.; Durcova, O.; Marcincin, A. Acta Polym 1990, 41, 64.
15. Liang, B. R.; White, J. L.; Spruiell, J. E.; Goswami, B. C. J Appl Polym Sci 1983, 28, 2011.
16. Moseley, W. W. J Appl Polym Sci 1960, 3, 266.
17. Gupta, B. S.; Whang, H. S. Int Nonwovens J 1999, 18, 36.
18. Ribbe, A. E. Trends Polym Sci 1997, 5, 333.
19. Nadella, H. P.; Henson, H. M.; Spruiell, J. E.; White, J. L. J Appl Polym Sci 1977, 21, 3003.
20. Samuels, R. J. Structured Polymer Properties. Wiley Interscience: New York, 1974.
21. Alexander, L. E. X-Ray Diffraction Methods in Polymer Science; Wiley Interscience: New York, 1969.
22. Samuels, R. J. J Polym Sci 1965, A3, 1741.
23. Private communication with Dr. Hawthorne Davis; Balcerzyk, E.; Kozlowski, W.; Wesolowska, E.; Lewaszkiewicz, W. J Appl Polym Sci 1981, 26, 2573.
24. Born, M.; Wolf, E. Principles of Optics; Pergamon Press: London, 1980.
25. Gonzalez-Montiel, A.; Keskkula, H.; Paul, D. R. J Polym Sci Part B: Polym Phys 1995, 33, 1751.
26. Leidner, J.; Woodhams, R. T. J Appl Polym Sci 1974, 18, 1639.
27. Nielsen, L. E. J Appl Polym Sci 1966, 10, 97.
28. Nielsen, L. E. J Compos Mater 1967, 1, 100.
29. Paul, B. Trans Metallurgy Soc AIME 1960, 218, 36.
30. Teli, M. D.; Ramani, V. Y.; Adivarekar, R. V. J Text Assoc 1996, 56, 205.
31. Afshari, M.; Kotek, R.; Haghighat Kish, M.; Nazock Dast, H.; Gupta, B. S. Polymer 2002, 43, 1331.
32. Saito, H.; Inoue, T. J Polym Sci Part B: Polym Phys 1987, 25, 1629.